An implosive component to the source of the deep Sea of Okhotsk earthquake of 24 May 2013: Evidence from radial modes and CMT inversion

Emile A. Okal[a,*], Nooshin Saloor[a], Stephen H. Kirby[b], Meredith Nettles[c]

[a] Department of Earth and Planetary Sciences, Northwestern University, Evanston, IL 60208, USA
[b] United States Gelogical Survey, Menlo Park, CA 94025, USA
[c] Lamont-Doherty Earth Observatory, Columbia University, Palisades, NY 10964, USA

A B S T R A C T

We study the spectral amplitudes of the first two Earth radial modes, $_0S_0$ and $_1S_0$, excited by the Sea of Okhotsk earthquake of 24 May 2013, the largest deep event ever recorded, in the search for an isotropic component to its source. In contrast to the case of the 1994 Bolivian earthquake, we detect an implosive component $M_I = -1.1 \times 10^{27}$ dyn*cm, equivalent to 3% of the full scalar moment, but 14% of the lone deviatoric component exciting the Earth's radial modes. An independent moment tensor inversion, using the standard GlobalCMT algorithm but after relaxing its zero-trace constraint, similarly yields an implosive isotropic component, albeit with a larger amplitude, while it fails to document one in the case of the 1994 Bolivian deep earthquake. An implosive component to the source is expected in the model of transformational faulting in which deep earthquake rupture nucleates and grows upon transformation of metastable olivine to ringwoodite in the cold subducting slab. This interpretation is supported by quantitative estimates (0.9–4 m) of the thickness of the transformed shear zone, which scale favorably, relative to earthquake fault length, with the upper end of the range of laboratory results reported for ices, germanates and silicates. The resulting extent of the transformation in the metastable wedge is consistent with the local geometry of the deep slab, as recently determined by rupture modeling and aftershock distribution. Our results are in contrast to those for the two runner-up largest deep earthquakes, the 1994 Bolivian and 1970 Colombian shocks, for which a similar isotropic component could not be detected. We attribute this difference to variability in the ratio of isotropic to deviatoric components, which combined with the smaller size of the 1970 and 1994 events, would make any putative implosive component fall below detection levels, especially in the case of the 1970 Colombian earthquake for which only analog narrow-band records were available.

1. Introduction and historical perspective

The existence of deep earthquakes was definitely proven by Wadati (1927, 1928, 1929), who noticed that for such events, it was impossible to reach their focus at distance zero, using observables at the surface of the Earth, such as S–P travel times or the increase of felt intensities in the epicentral area. This remarkable observation reopened the question of the origin of seismogenesis at great depths, where high temperatures and pressures would *a priori* exclude the possibility of brittle rupture, an argument forcibly used by Jeffreys (1924) to counter earlier and less robust suggestions of deep seismicity (Pilgrim, 1913; Mainka, 1915; Turner, 1922).

In this context, Bridgman (1945) first proposed that phase transitions could play a role in the mechanism of deep earthquakes, even though studies such as Stechschulte (1932) or Leith and Sharpe (1936)

had argued for a largely common mechanism of rupture (a "consanguinity" in the latter's terms) between deep and shallow earthquakes. Indeed, a most remarkable result of modern seismology has been that focal mechanisms of deep earthquakes could be modeled, at least to an excellent approximation, by double couples, *i.e.*, by the same representation as their shallow counterparts (*e.g.*, Isacks and Molnar, 1971). In this context, the role of a phase transition might be only that of a component to the focal mechanism, possibly a small one (Vaišnys and Pilbeam, 1976), meaning that it might be detected only during very large deep events, the latter being of course comparatively rare.

A phase transformation at the source should involve a change in volume, and hence an isotropic component to its moment tensor. Using a systematic inversion of hand-digitized analog seismograms from the 1963 Peru-Bolivia and 1970 Colombia deep shocks, Gilbert and Dziewonski (1975) first proposed that they did indeed feature an

* Corresponding author.
  E-mail address: emile@earth.northwestern.edu (E.A. Okal).

implosive component (as large as 40% of the deviatoric one), but Okal and Geller (1979) later suggested, and Russakoff et al. (1997) proved, that their result was an artifact of various simplifications in both the Earth model used and the inversion algorithm. With the advent of digital data, it became possible to explore the source of smaller events, and a review of 19 deep shocks by Kawakatsu (1991a) failed to identify any isotropic component to their moment, with a threshold of detection of 10% of the full moment.

The occurrence of the 1994 Bolivian deep earthquake whose moment, 2.8×10^{28} dyn*cm, was twice that of the 1970 Colombian shock, motivated a number of systematic searches for an isotropic component to the moment tensor, which however, returned either no such evidence (Hara et al., 1995; Okal, 1996), or a suggestion marred by systematic trade-offs (Kikuchi and Kanamori, 1994). The conclusion of these studies was that any isotropic component had to be small enough to evade detection, and thus had to represent at most a nucleation of the principal element of stress release, the latter taking place through a process essentially equivalent to the source of shallow earthquakes, represented by a pure double-couple.

This concept is in general agreement with the model of "transformational faulting", in which rupture nucleation and growth accompany the phase transformation of olivine that persists in a metastable state, due to unfavorable kinetics in the cold subducting slab (Kirby, 1987; Kirby et al., 1991; Kirby et al., 1996). The emission of acoustic energy upon transformation of metastable materials has been observed in the laboratory on samples of ices (Kirby et al., 1991), germanates (Green and Burnley, 1989; Burnley et al., 1991) and forsterite (Green et al., 1990; Wang et al., 2017). The rupture nucleation process has been referred to as "anti-cracking" by Green and Burnley (1989) and Green et al. (1990). The olivine wedge inside the subducted Western Pacific slab has recently been imaged in the Southwest Japan and Mariana slabs using receiver function techniques (Kaneshima et al., 2007; Kawakatsu and Yoshioka, 2011), and below the Sea of Japan and Northeastern China using seismic tomography (Jiang et al., 2015).

In this context, the occurrence of the Sea of Okhotsk deep earthquake of 24 May 2013 provides a new opportunity to conduct an in-depth search for an isotropic component to its moment tensor. At $M_0 = 3.95 \times 10^{28}$ dyn*cm, this event is the largest deep earthquake ever recorded, its moment being 1.4 times that of the 1994 Bolivian earthquake (Fig. 1), and incidentally, the eighth-largest regardless of depth in the GlobalCMT catalog. In the present paper, we apply the analysis of Okal (1996) to the 2013 event and, this time, document the presence of a resolvable implosive component M_I amounting to 3% of the deviatoric moment. We confirm this result, albeit with a larger value for M_I, through unconstrained moment tensor inversions using a variation of the GlobalCMT algorithm.

2. Methodology

A significant problem in the detection of an isotropic component M_I to the moment tensor **M** is that it can trade off with other, deviatoric, ones during the inversion of observable seismic waveforms. While Kawakatsu (1996) showed that M_I can in principle be resolved from the spectra of classical spheroidal modes at frequencies less than 2 mHz, Okal (1996) elected to focus on the spectral amplitudes of the two radial modes $_0S_0$ and $_1S_0$. The advantage of this approach stems from the fact that in radial modes the non-diagonal elements of the eigenstrain are identically zero, and additionally $\varepsilon_{\theta\theta} = \varepsilon_{\phi\phi} = \frac{u_r}{r}$, leaving only two independent non-zero components of the strain tensor. Since the excitation of any mode by a moment tensor **M** is proportional to its scalar product with the eigenstrain at the source (Gilbert, 1971), it follows that radial modes are excited by only two independent components of a general 6-dimensional symmetric moment tensor, which can be taken as $M_I = \frac{1}{3} M_{ii}$, and $[M_{rr}-(M_{\theta\theta} + M_{\phi\phi})/2]$, in principle resolvable from the inversion of just two radial mode amplitudes.

The combination $[M_{rr}-(M_{\theta\theta} + M_{\phi\phi})/2]$ is equivalent to $-3/2$ times the vertical CLVD component of Kawakatsu's (1996) decomposition of the most general moment tensor **M**. If we then assume the deviatoric part of the source to be a pure double-couple, this combination also takes the form $M_D \cdot s_R$, where M_D is the moment of the double-couple, and $s_R = \sin\lambda\sin\delta\cos\delta$ in the notation of Kanamori and Cipar (1974), is a trigonometric coefficient expressing the component of thrusting ($s_R > 0$) or normal faulting ($s_R < 0$) in the deviatoric source. The excitation of the radial mode is then proportional to $[N_0 \cdot M_I + K_0 \cdot M_D s_R]$, where N_0 and K_0 are two excitation coefficients depending only on source depth. As discussed by Okal (1996), and for the deepest
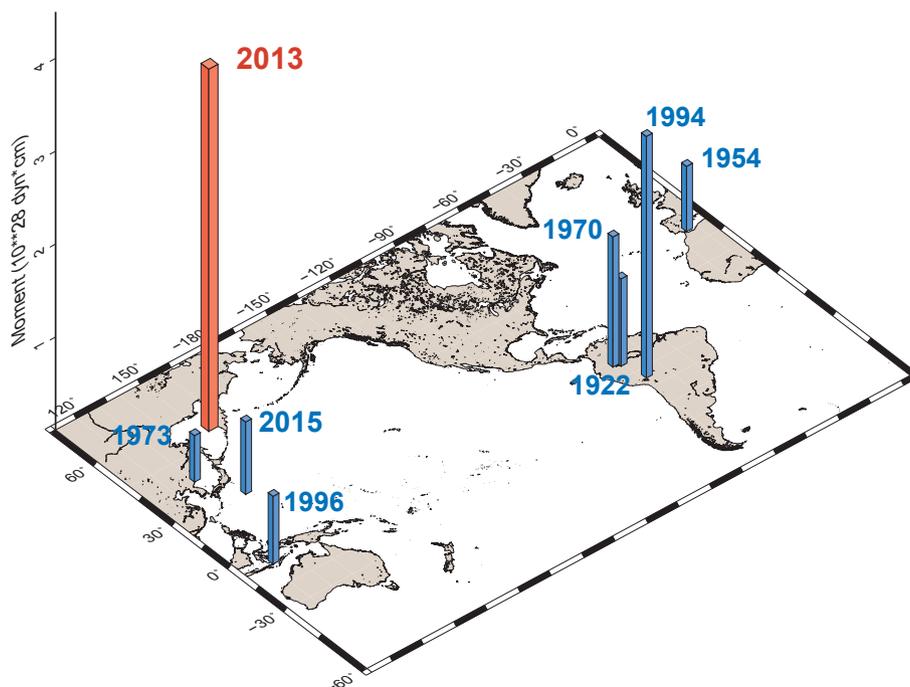
Fig. 1. Sketch of the only eight deep events ($h > 400$ km) known since 1900 with measured moments $M_0 \geqslant 5 \times 10^{27}$ dyn*cm. The bars are scaled to moment.

earthquake sources, the modes $_0S_0$ and $_1S_0$ are particularly suited to this inversion, since the two excitation coefficients are comparable for $_1S_0$ ($_1K_0 = -0.094; _1N_0 = -0.115$) and of comparable amplitude but opposite signs for $_0S_0$ ($_0K_0 = 0.280; _0N_0 = -0.313$; all values in units of 10^{-31}, using the PREM model (Dziewonski and Anderson, 1981) and the GlobalCMT centroid depth of 611 km). This makes the inversion matrix very well-behaved, with complex conjugate eigenvalues and hence a condition number of 1. This property (which was essentially unchanged at the 1994 Bolivian shock's depth of 640 km) allowed Okal (1996) to solve for M_I independently of the deviatoric component $M_D \cdot s_R$, and to conclude that no resolvable M_I could be identified in the source of the 1994 Bolivian earthquake.

3. Results: evidence for an implosive component

3.1. Preliminary investigation: the spheroidal modes

Following our earlier investigations of the 2004 Sumatra, 2005 Nias, 2010 Maule and 2011 Tohoku events (Okal and Stein, 2009; Okal et al., 2012; Okal, 2013), we first conducted a systematic study of the excitation of spheroidal modes by the 2013 deep Sea of Okhotsk earthquake, in the range 0.63–2.70 mHz, with the aim of documenting any possible source slowness. The great depth of the 2013 event allows the systematic use of many spheroidal overtones.

We recall that, given a focal mechanism geometry, this procedure consists of computing the excitation of each split singlet $_nS_l^m$ within a multiplet $_nS_l$ at each station (Stein and Geller, 1977), producing a synthetic record and scaling its spectrum to the observed one to derive a value of the seismic moment at the relevant frequency; all details can be found in Okal et al. (2012). Fig. 2 shows that no trend is present in the spectrum of the 2013 Sea of Okhotsk earthquake, with the gravest mode resolvable, $_0S_4$ ($T = 1565$ s), yielding a moment not significantly different from that of the GlobalCMT solution obtained at 200 s. This result, in contrast to the case of the 2004 Sumatra earthquake (Stein and Okal, 2005; Okal and Stein, 2009), means that in the range of frequencies considered, the stress release can be regarded as a step function in time. Its importance is that it precludes interpreting any anomalous spectral amplitudes of the radial modes $_0S_0$ and $_1S_0$ as simply due to source slowness, and any such behavior must then be explained by an ancillary component to the moment tensor.

3.2. The radial modes

For the present study, we recover the spectra of the radial modes $_0S_0$ and $_1S_0$ from time series of VHZ channels at stations of the GEOSCOPE and Global Seismological networks. As discussed by Dahlen (1982), the proper resolution of a spectral line of period T and quality factor Q requires a time series lasting on the order of ($T \cdot Q/2$), or 40 days for $_0S_0$ and 7 days for $_1S_0$, using $Q = 5579$ and 2017, respectively (Okal and Stein, 2009). We note that a somewhat deep earthquake ($h = 386$ km) with a moment of 1.1×10^{27} dyn*cm occurred in the Solomon Islands on 07 July 2013, 44.5 days after the Okhotsk event, with a normal faulting mechanism favorable for the excitation of radial modes. For this reason, we use only 40-day time windows. We retain only records unperturbed by gaps or spikes over the relevant windows, leaving us with a dataset of seven stations: ADK, CAN, IVI, KMB, MAKZ, NNA, and PAYG.

Since the particle displacements of the radial modes are the same at all points on the surface of the Earth, it is possible to stack their complex spectra at the various stations to improve signal-to-noise ratios. Fig. 3 presents the final stacked spectra (using simple, unweighted stacking) for the fundamental $_0S_0$ and first overtone $_1S_0$. The moment values reported on the figures represent the best fits obtained under the assumption of a purely deviatoric source in the geometry of the GlobalCMT best double-couple ($\delta = 11°$, $\lambda = -93°$). It is immediately evident that, with respect to the GlobalCMT solution ($M_0 = 3.95 \times 10^{28}$ dyn*cm), the moment obtained for $_0S_0$ is significantly deficient (by 15% at only 3.42×10^{28} dyn*cm), while that for $_1S_0$ is similarly excessive (by 21% at 4.77×10^{28} dyn*cm). We will refer to these values of the moment as $_0m$ and $_1m$, respectively.

On the other hand, if we assume that the source is composed of a double-couple with the GlobalCMT geometry (and moment M_D), plus an isotropic component of moment M_I, then M_I and M_D can be resolved from the system of equations

$$\begin{bmatrix} _0N_0 & _0K_0 \\ _1N_0 & _1K_0 \end{bmatrix} \begin{bmatrix} M_I \\ M_D s_R \end{bmatrix} = \begin{bmatrix} _0m \cdot _0K_0 s_R \\ _1m \cdot _1K_0 s_R \end{bmatrix} \quad (1)$$

whose solution is $M_I = -1.08 \times 10^{27}$ dyn*cm and $M_D = 4.06 \times 10^{28}$ dyn*cm. Thus, the excitation of the radial modes is explained by the superposition of a deviatoric moment essentially identical to the GlobalCMT solution, and a negative isotropic (i.e., implosive) component M_I amounting to 3% of the deviatoric one (but as much as 14% of the deviatoric component relevant to the excitation of normal modes, $M_D s_R = -7.60 \times 10^{27}$ dyn*cm).

Following Okal's (1996) approach, we obtain estimates of error bars
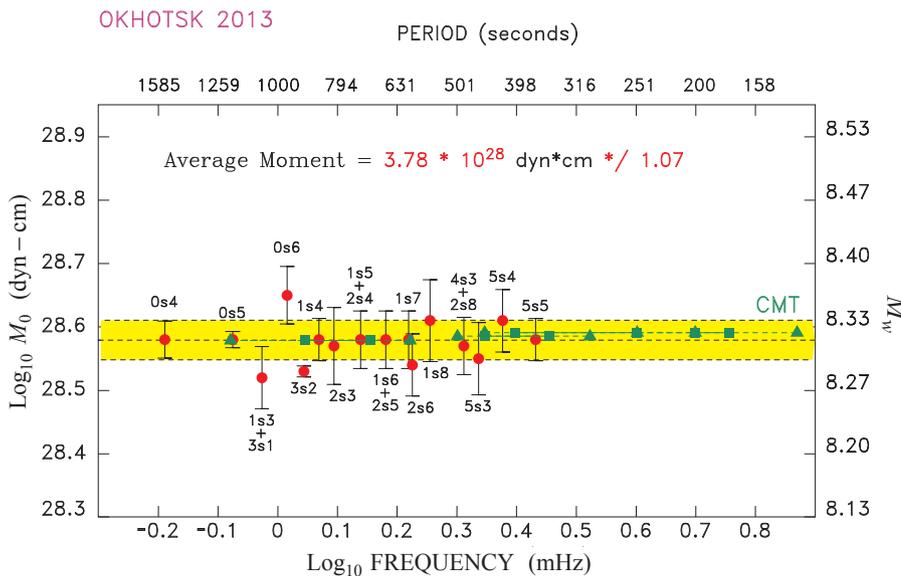
Fig. 2. Seismic moment of the 2013 Sea of Okhotsk deep earthquake computed from the spectra of the Earth's spheroidal modes. For each mode, the moment is obtained by fitting the observed spectrum of the multiplet to its theoretical shape in the geometry of the GlobalCMT solution. The geometrical average for all usable stations is shown as the red dot, with corresponding standard deviation. The dashed line (and colored band) represent the average value (and standard deviation) of these moments at the various frequencies. Note the absence of any trend with frequency, contrary to the case of the 2004 Sumatra earthquake (Okal and Stein, 2009; Fig. 7). Shown in green are results of unconstrained CMT inversions in various frequency bands, as listed in Table 1 and discussed in Section 4; triangles and squares define the cut-off and taper limits, respectively, of the filters used for each band. Note full consistency of results. (For interpretation of the references to colour in this figure legend, the reader is referred to the web version of this article.)
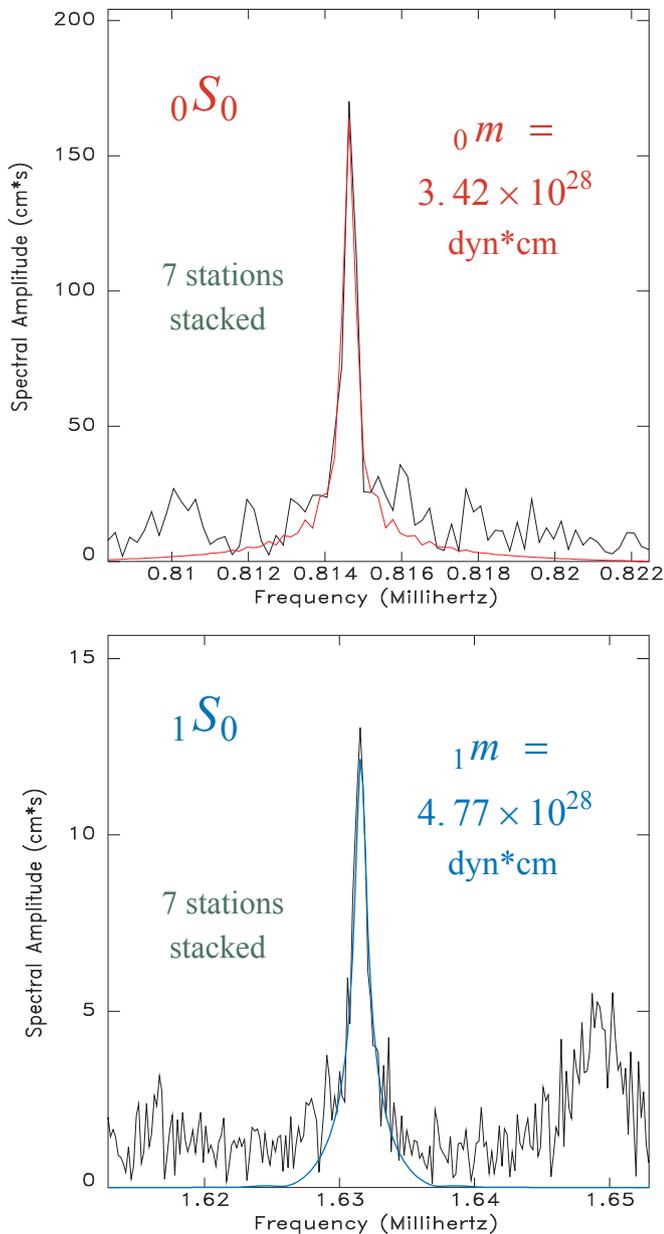
Fig. 3. Best fits to the stacked spectra of $_0S_0$ *(Top)* and $_1S_0$ *(Bottom)*, under the assumption of a purely deviatoric source in the geometry of the GlobalCMT solution. In both frames, the black trace is the observed stacked spectrum, and the colored one its theoretical fit for the computed moment. (For interpretation of the references to colour in this figure legend, the reader is referred to the web version of this article.)

Fig. 4. Isotropic and deviatoric components of the source of the 2013 Okhotsk (red) and 1994 Bolivia (green) events, inverted from the spectra of the radial modes $_0S_0$ and $_1S_0$. The error ellipses are obtained from the jackknifing procedure. The 1994 data was simply replotted from Fig. 2 of Okal (1996), using a common scale. Note the robust character of the 2013 solution, contrary to the 1994 case, where even the polarity of the isotropic component could not be asserted. (For interpretation of the references to colour in this figure legend, the reader is referred to the web version of this article.)

on M_I and M_D through a jackknifing procedure consisting of running $N = 7$ inversions from stacks of $N-1$ stations (eliminating one common station at a time), and fitting an ellipse to the resulting dataset in the $[M_I, M_D]$ space. Results are shown on Fig. 4, together with those for the 1994 Bolivian earthquake, replotted on a common scale from Fig. 2 of Okal (1996). They suggest an uncertainty of 11% on M_I and 2% on M_D, which emphasizes the robust character of the isotropic component. By contrast, and as recalled on Fig. 4, in the case of the 1994 Bolivian earthquake, the isotropic component was not robust, with the ellipse intersecting the neutral line $M_I = 0$, meaning that the dataset was inconclusive as to even the sign of any putative isotropic component (implosion or explosion). We thus conclude that the 2013 Okhotsk Sea earthquake does possess an implosive isotropic component, on the order of 3% of the deviatoric moment M_D.

Finally, we note that the inclusion of a relatively small isotropic component to the moment tensor cannot affect significantly the inversion for the best-fitting double-couple, since the isotropic term excites only the $m = 0$ singlet of each mode. In the particular geometry of the deep Sea of Okhotsk earthquake (a décollement on a plane dipping only 11°), the $m = 0$ singlet is only marginally excited by the deviatoric tensor, and thus the geometry and scalar moment of the best-fitting double-couple is essentially unaltered by the addition of M_I. In other words, the small isotropic component excites only marginally the main seismological observables (*i.e.,* the mantle Rayleigh waves or the non-radial modes) which are essentially unaffected by its presence, a result already described by Okal and Geller (1979).

3.3. The case of the 2015 Bonin earthquake

A surprising, large deep earthquake took place at the bottom of the Bonin Islands Wadati-Benioff Zone on 30 May 2015 (27.94°N; 140.56°E; Fig. 1). With a seismic moment of 7.7×10^{27} dyn*cm, this earthquake is the third largest deep event in the GlobalCMT catalog (after the 2013 Okhotsk and 1994 Bolivian shocks). Several properties make it particularly intriguing (Okal and Kirby, 2016; Ye et al., 2016): First, estimates of its source depth place it at 664 km (hypocentral, NEIC), 682 km (hypocentral, JMA), 667 km (hypocentral, Zhao et al. (2017)), and 681 km (centroid, GCMT), in rough numbers 100 km deeper than all seismicity previously known in that segment of the subduction system; next, it did not take place in the linear prolongation of the seismic zone, but rather 200 km East of it, *i.e.,* oceanwards of the downgoing slab; finally, its focal mechanism features tensional stress in the direction of sinking of the slab, rather than the usual down-dip compression characteristic of stress release at the bottom of slabs (Isacks and Molnar, 1971). All these properties fuel speculation (Okal and Kirby, 2016) as to whether the event took place in a mechanically

detached section of slab recumbent on the bottom of the transition zone (Okal and Kirby, 1998; Okal, 2001) or in a highly contorted one. Detailed tomography of the Bonin slab system by Zhao et al. (2017, Figs. 4 and 6) would suggest a tear in the slab around 29°N, with the Southern segment curling back oceanwards, perhaps in conjunction with the further Eastward regression of the subduction in the Marianas to the South, in the general geometry suggested by Čížková and Bina's (2015) geodynamic models. In Zhao et al.'s (2017) model, and at the latitude of the 2015 event, the slab squeezes through a narrow neck at the level of the 410-km discontinuity, followed by an effusive outpouring down to ~ 850 km, which would contain the 2015 hypocenter (their Fig. 4); the wide expansion of the slab below the 410-km neck, as opposed to its abutting against the 660-km discontinuity, may also help explain the unusual down-dip tensional mechanism. On the other hand, the isolated character of the 2015 earthquake would argue in favor of its occurrence in a mechanically detached portion of slab, recumbent on the 660-km discontinuity (Okal and Kirby, 2016), and where the orientation of stresses released seismically could be essentially random, as observed in the deep seismic cluster under the Fiji Basin (Okal and Kirby, 1998).

Given its large moment, and regardless of the exact environment of the 2015 Bonin earthquake, it would then become a natural suggestion to investigate its radial modes, to explore the possible presence of an isotropic component in its source. Unfortunately, the 2015 earthquake was just too small to sufficiently excite the radial modes, and we simply failed to extract either $_0S_0$ or $_1S_0$ above noise level.

4. Verifying the robustness of M_I

Given the historical controversy attached to the question of the isotropic component of deep earthquakes, it is important to examine the robustness of our results in view of some of the simplifying assumptions underlying our methodology, which for example ignores lateral heterogeneity in the Earth's structure.

4.1. Possible artifacts for radial mode measurements

We first address the robustness of our results with respect to the Earth model used, by using a different laterally homogeneous Earth model, namely 1066A (Gilbert and Dziewonski, 1975). We find negligible changes in the result of the inversion (1) (less than 0.1% in M_D and 1.5% in M_I).

Next, we recall that Okal and Geller (1979) studied the effect of ignoring lateral heterogeneity in Earth structure on moment tensor inversion, showing that the introduction of a simple degree-two perturbation in the phase velocity of synthetic surface waves, followed by inversion using a laterally homogeneous model, was enough to add an artificial isotropic component to an otherwise deviatoric source. They suggested that the large isotropic component to the source of the 1970 Colombian event proposed by Gilbert and Dziewonski (1975) resulted from such an artifact. In simple terms, by using a slightly inappropriate phase velocity, this effect amounts to introducing an improper time shift between the various records used in the inversion. In the present case, and since the radial modes involve no propagation (their "phase velocity" being infinite), this effect is not expected to take place.

As discussed by Russakoff et al. (1997), a more complex situation may arise from mode-to-mode coupling, due to the combined effects of the Earth's rotation, ellipticity and lateral heterogeneity. In particular, those authors showed that the former was most probably responsible for the isotropic component proposed by Gilbert and Dziewonski (1975) for the 1970 event, which disappeared below detection level once this "Coriolis coupling" effect was properly taken into account. Briefly stated, coupling can deform the eigenfunction of a mode (*e.g.,* a toroidal mode may acquire a small radial component to its displacement), which in turn affects its excitation coefficients by various moment tensor components, and hence perturbs the result of the inversion. As detailed theoretically by Woodhouse (1980), Coriolis and ellipticity coupling

will be significant between (i) spheroidal modes of identical angular degree *l*; and (ii) modes of different type (one spheroidal, one toroidal) whose degrees *l* differ by 1. In addition (iii), ellipticity may couple modes of the same kind (*S* or *T*) with degrees differing by 2. In all cases, efficient coupling between two modes requires that the difference in their unperturbed multiplet frequencies be comparable to the range of splitting induced by the perturbation; we stress that this identity of frequency between two modes required for efficient coupling must occur in the complex domain, *i.e.* taking into account the imaginary part of the eigenfrequency induced by anelastic attenuation. The exceptionally high values of *Q* for the radial modes (5579 and 2017 respectively for $_0S_0$ and $_1S_0$) act to further minimize the possibility of coupling to non-radial modes. Incidentally, type (i) coupling requires that two branches of physically different *S* modes cross each other (Okal, 1978).

Millot-Langet (2004) has introduced a Frobenius normalization of the coupling between two modes indexed *k* and *k'* through the quantifier

$$F_{kk'} = -\log_{10}\left|\frac{\langle\mathbf{v}_k|\delta\mathbf{H}|\mathbf{u}_{k'}\rangle}{\omega_k^2-\omega_{k'}^2}\right|$$

(2)

where $\langle\mathbf{v}_k|$ and $|\mathbf{u}_{k'}\rangle$ are "bra" and "ket" descriptions of orthonormalized eigenfunctions for modes *k* and *k'*, and $\delta\mathbf{H}$ the perturbation induced by rotation and ellipticity on the Hamiltonian operator. In general, coupling with *F* values on the order of 2 or greater is deemed negligible.

Here, we consider the radial modes $_pS_0$ (*p* = 0 and 1), whose frequencies closely follow $_p\omega_0 = (p+1)_0\omega_0$; they will clearly be immune to (i). Type (ii) coupling would require a toroidal mode $_nT_1$ with a period approaching either 1227 or 613 s, which we can exclude given the periods of $_0T_1$ (solid rotation, infinite period), $_1T_1$ (807 s) and $_2T_1$ (456 s); at any rate, a detailed examination of the structure of the coupling kernels (*e.g.,* Millot-Langet (2004)) shows that they vanish at first order for all coupling of the form $_pS_0-_nT_1$. As for (iii), the closest candidate for coupling with $_1S_0$ would be $_4S_2$ (*T* = 580 s). Using the parameters listed by Dahlen and Sailor (1979), we find that the width of its split multiplet is 0.006 mHz, 15 times smaller than its difference in frequency with $_1S_0$; the resulting coefficient $F_{_1S_0\,_4S_2}$ is 1.92. For $_0S_0$, the closest contenders would be $_1S_2$ (*T* = 1470 s) and $_2S_2$ (*T* = 1057 s). For the former, its split width is similarly 0.011 mHz, or 12 times its distance to $_0S_0$ in the frequency domain, and $F_{_0S_0\,_1S_2}$ = 2.14. The latter is an inner core mode ($_1K_2$ in Okal's (1978) classification), hardly excited by any earthquake at any depth, and whose singlets are mixed with those of $_3S_1$ and $_1S_3$; the Frobenius coefficient $F_{_0S_0\,_2S_2}$ is 3.22. We conclude that the effect of coupling induced by rotation and ellipticity on the first two radial modes is negligible.

Another possible effect leading to the observation of an artificial isotropic component could be structural anisotropy at the source, as discussed *e.g.,* by Kawasaki and Tanimoto (1981) and later Vavryčuk (2005). However, in an investigation of events at ridge-transform intersections showing significant minor double-couples, Kawakatsu (1991b) has shown that the latter could not be explained by structural anisotropy at the source, even though such environments are known to feature strong and coherent anisotropy. In addition, Vavryčuk (2004) has suggested that the level of anisotropy necessary to account for observed CLVD components at the bottom of the Tonga slab would translate into an artificial isotropic component of about 1%. We conclude that it is unlikely that our observation of an implosive component of 3% of M_D is an artifact of anisotropy.

4.2. Unconstrained CMT inversions: an independent approach

In an independent approach, we proceed to verify our detection of an implosive component to the 2013 Okhotsk earthquake through 6-dimensional centroid-moment tensor inversions unconstrained to a

Table 1
Results of Moment Tensor Inversion Experiments: 2013 Sea of Okhotsk.

No.	Centroid				Inverted Moment Tensor							Best Double-Couple				M_I		ε	ε_D
	Lat. (˚N)	Lon. (˚E)	Depth (km)	Offset (s)	M_{rr}	$M_{\theta\theta}$	$M_{\phi\phi}$	$M_{r\theta}$	$M_{r\phi}$	$M_{\theta\phi}$	Residual	M_D	ϕ (°)	δ (°)	λ (°)	(%)†			
							2013 OKHOTSK: Standard Inversion												
1c	54.61	153.77	611	19.35	−1.67	0.382	1.28	−0.784	−3.57	0.155	0.0891	3.94	188.6	11.1	−93.5	0			−0.087
2u	54.61	153.82	607	19.34	−1.89	0.026	0.960	−0.783	−3.54	0.158	0.0888	3.90	188.2	10.8	−94.0	**−0.301**	**(−7.7)**	−0.0007	−0.075
							Improved Station Dataset												
3c	54.61	153.79	611	19.38	−1.69	0.372	1.31	−0.789	−3.57	0.128	0.0971	3.96	186.2	11.3	−95.8	0			−0.087
4u	54.61	153.84	606	19.37	−1.94	−0.0271	0.946	−0.787	−3.54	0.134	0.0967	3.91	185.8	11.0	−96.2	−0.340	(−8.7)	+0.087	−0.117
							Remove Cross-Branch Stations												
5c	54.59	153.78	610	19.40	−1.69	0.415	1.27	−0.807	−3.57	0.206	0.0791	3.95	192.9	11.2	−89.9	0			−0.089
6u	54.59	153.83	606	19.40	−1.94	0.0153	0.902	−0.806	−3.54	0.210	0.0782	3.90	192.6	10.9	−90.2	−0.341	(−8.7)	+0.007	−0.267
							Short-Period Window 135–250 s												
7c	54.68	153.73	611	20.61	−1.47	0.334	1.14	−1.00	−3.54	0.142	0.1205	3.91	188.0	9.9	−97.3	0			−0.078
8u	54.68	153.76	611	20.61	−1.74	0.0228	0.837	−1.00	−3.54	0.146	0.1200	3.90	187.9	9.8	−97.4	−0.293	(−7.5)	−0.001	−0.102
							Long-Period Window 300–500 s												
9c	54.64	153.80	611	18.57	−1.76	0.352	1.40	−0.503	−3.51	0.147	0.0968	3.89	187.7	12.1	−90.4	0			−0.082
10u	54.64	153.90	604	18.57	−1.92	0.106	1.20	−0.507	−3.48	0.149	0.0966	3.85	187.3	12.0	−90.9	−0.205	(−5.3)	−0.021	−0.073
							Ultra-Long-Period Window 600–1200 s												
11c	54.44	152.63	597	19.75	−1.55	0.450	1.10	−0.811	−3.39	0.131	0.2580	3.74	190.8	10.5	−92.4	0			−0.108
12u	54.39	153.00	576	19.60	−2.02	0.224	0.914	−0.826	−3.39	0.145	0.2573	3.79	191.3	11.5	−92.2	−0.294	(−7.6)	−0.045	−0.121
							Ultra-Long-Period with Longer Records												
13c	54.40	152.23	602	22.10	−1.61	0.502	1.11	−0.850	−3.31	0.148	0.2677	3.68	192.9	11.0	−91.3	0			−0.120
14u	54.34	152.57	580	21.90	−2.06	0.285	0.926	−0.862	−3.31	0.162	0.2670	3.74	193.4	11.9	−91.1	−0.283	(−7.6)	−0.058	−0.132

All moment values in units of 10^{28} dyn*cm.

  † Value of M_I/M_D expressed in percent.

zero-trace condition. The procedure consists of running the inversion algorithm applied to the routine computation of GlobalCMT solutions (Dziewonski et al., 1981; Ekström et al., 2012), but after relaxing the zero-trace constraint imposed in its standard version. This yields a six-dimensional symmetric moment tensor **M**, rather than a five-dimensional one. Table 1 compares the results of both inversions. The first solution, 1c (for constrained), reproduces the entry of the 2013 Okhotsk event in the standard GlobalCMT catalog. The second solution, 2u (for unconstrained), features a trace $M_{rr} + M_{\theta\theta} + M_{\phi\phi} = -9.04 \times 10^{27}$ dyn*cm, corresponding to $M_I = -3.01 \times 10^{27}$ dyn*cm. The best double-couple is then computed in the standard way, after obtaining the new deviatoric five-dimensional tensor by subtracting from the six-dimensional **M** the isotropic component $M_I \cdot \mathbf{I}$ where **I** is the identity matrix. The last two columns of Table 1 express the so-called "Compensated Linear Vector Dipole" characterizing the relative importance of the moment tensor components remaining after subtraction of the best-fitting double-couple, through the parameter

$$\varepsilon = \frac{\lambda_{\mathrm{int}}}{\max[\lambda_{\max}, -\lambda_{\min}]} \qquad (3)$$

which is the ratio of the intermediate eigenvalue of the moment tensor (zero for a pure double-couple) to the one of largest absolute value. In Table 1, ε refers to the full six-dimensional tensor and ε_D to its deviatoric part; they are obviously equal in the constrained inversion.

The most important result in Solution 2u is that $M_I = -0.30 \times 10^{28}$ dyn*cm, is *negative*, corresponding to an implosion and supporting our radial mode results. However, its amplitude is found to be about 2.8 times larger. Other important results concern the robustness of the centroid location (which moves less than 5 km in 3 dimensions), and of the centroid time offset (which changes by an insignificant 0.01 s, less than the time sampling of the data used, and hence than the precision of the algorithm); however, the quality of the solution achieved improves only marginally, by less than 1%. The geometry of the best double-couple is also changed less than 1° in all angles, and its moment is reduced by only 1%.

The robustness of the inversion results is further examined by altering details of either the dataset or the parameters of the algorithm. In Solutions 3c (constrained) and 4u (unconstrained), we exclude stations whose response characteristics may be questionable, but on the other hand include data from other networks, such as GEOSCOPE, MEDNET or GEOFON; in Solutions 5c and 6u, we exclude components involving cross-branch coupling visible in the time domain. In the next experiments, we alter the period band over which the inversion is carried (originally 200–400 s in Solutions 1–6). First, we reproduce the shorter-period band (135–250 s) used in the CMT algorithm prior to 2004 (Solutions 7c (constrained) and 8u (unconstrained)). On the opposite, we consider a long-period band (300–500 s; Solutions 9c and 10u), and even an ultra-long-period one (600–1200 s; Solutions 11c and 12u). Finally, for Solutions 13c and 14u, we consider the ultra-long-period band, but with extended time windows.

Table 1 lists all details of the various solutions. We note that, with the exception of the long-period experiment (300–500 s), all inverted moment components remain remarkably stable, featuring a standard deviation of less than 0.12×10^{28} dyn*cm. Consequently, the isotropic component also remains robust, at $(-0.308 \pm 0.023) \times 10^{28}$ dyn*cm. The best-fitting double-couples are also rotated at most 3° from each other in the formalism of Kagan (1991). However, in the long-period experiment (Solution 10u), most components, and in particular $M_{\phi\phi}$ and $M_{r\theta}$, feature large deviations of up to 30%, that in turn impact the isotropic component, which falls by about one third, to -0.21×10^{28} dyn*cm, or only −5.3% of M_D; the best fitting double-couple rotates by a Kagan angle of 7°. The deviatoric moment M_D also varies slightly (by about 2%), but, as shown on Fig. 2, remains within the standard deviation of the values inverted from ultra-long-period spheroidal modes (see 3.1 above).

Table 2
Results of Moment Tensor Inversion Experiments: 2015 Bonin Islands event.

No.	Centroid				Inverted Moment Tensor							Best Double-Couple				M_I		ε	ε_D
	Lat.	Lon.	Depth	Offset	M_{rr}	$M_{\theta\theta}$	$M_{\phi\phi}$	$M_{r\theta}$	$M_{r\phi}$	$M_{\theta\phi}$	Residual	M_D	ϕ	δ	λ				
	(°N)	(°E)	(km)	(s)									(°)	(°)	(°)		(%) [†]		
							2015 BONIN ISLANDS: Standard Inversion												
15c	27.94	140.56	681	8.94	−0.386	−0.0657	0.452	−0.287	0.561	0.110	0.1918	0.765	35.6	24.8	−38.8	0			−0.077
16u	27.93	140.55	680	8.95	−0.414	−0.101	0.417	−0.287	0.558	0.109	0.1917	0.761	35.7	24.8	−38.5	**−0.033**	**(−5.1)**	−0.033	−0.075
							Short-Period Window 135–250 s												
17c	27.90	140.56	679	9.21	−0.383	−0.0740	0.457	−0.260	0.541	0.102	0.1691	0.742	35.0	25.2	−40.4	0			−0.050
18u	27.90	140.55	679	9.22	−0.424	−0.113	0.419	−0.260	0.540	0.101	0.1688	0.741	34.9	25.2	−40.5	−0.039	(−5.4)	+0.002	−0.050

All moment values in units of 10^{28} dyn*cm.
[†] Value of M_I/M_D expressed in percent.

We similarly examined the 2015 Bonin Islands event (Table 2) and the 1994 Bolivian earthquake (Table 3). In the former case, our results are comparable to those of the 2013 Okhotsk source: unconstrained inversions result in a small implosive component, amounting to ~ 5% of M_D (in absolute value); furthermore, the inversion results are robust, *i.e.,* they do not depend on the frequency window used in the inversion, and the value of M_D is unaffected by the nature of the inversion (constrained or unconstrained). However, the situation is different in the case of the 1994 Bolivian event. As shown in Table 3, inversions performed at short periods (135–250 s; Solution 20u) yield a negligible isotropic component, but at longer periods (200–400 s; Solution 22u), an implosive $M_I = -0.265 \times 10^{28}$ dyn*cm is obtained, equivalent to −7.7% of M_D, a ratio similar to that obtained for Okhotsk; in addition, while the best-fitting double-couple rotates only by a Kagan angle of 7°, its scalar value M_D increases significantly (by about 30%). At much longer periods (Inversion 24u), the value of M_D decreases back towards its short-period value, and the isotropic component disappears. Constrained inversions (19c, 21c, 23c) feature the same behavior of M_D. These results are summarized on Fig. 5 which analyzes them in the context of a quantification of ultra-low-frequency spheroidal modes of the Bolivian earthquake. Note that, as in the case of the Okhotsk event (Fig. 2), the mode results do not exhibit a trend with frequency suggestive of source slowness, and are compatible with the published CMT solution, which was obtained with a filter similar to the 135–250 s filter used here. However, the moment M_D for Solution 22u falls outside the standard deviation band, which does include the values obtained for Solutions 20u and 24u.

The inversion results for the Bolivian event are similar to those of Russakoff et al. (1997) for the 1970 Colombian deep shock: as shown *e.g.,* on their Fig. 7, those authors were unable to document an isotropic component outside the 2.5–3.5 mHz range, where mode-to-mode coupling (under scenario (ii) above) does takes place, but inversions ignoring that effect produced an artificial M_I. In this context, we elect to disregard from the present study all inversion results in the "Coriolis frequency band" and conclude that, as in the case of the 1970 Colombian earthquake, unconstrained CMT inversions of the 1994 Bolivian event do not yield a resolvable isotropic component, thereby confirming Okal's (1996) results using radial modes. This is in contrast to the case of the 2013 Okhotsk earthquake, for which all results obtained outside the Coriolis frequency band show a robust implosive component.

We conclude that the unconstrained CMT inversions support the essential difference in the sources of the two events evidenced by our radial mode studies, namely the presence of an implosive component in Okhotsk, and its absence in Bolivia. However, we presently have no explanation for the different amplitudes of M_I from CMT inversions and radial modes, especially given the good agreement between the corresponding values of M_D. Similarly, in the Coriolis frequency band, we lack a simple explanation for the relative weakness of the perturbations observed in the Okhotsk solution, as compared to the substantial ones

for Bolivia.

Finally, we note that our results are confirmed by recent work by Hara and Kawakatsu (2016), who detected an implosive component amounting to ~ 3% of the total moment tensor for the 2013 Sea of Okhotsk earthquake, but none above noise level for both the 1994 Bolivian and 2015 Bonin events. These authors, who used a CMT inversion technique, further documented the robustness of their results with respect to lateral heterogeneity in Earth structure.

5. A possible interpretation

In this section, we use the approach of Kirby et al. (1992) in an attempt to quantify the episode of phase transformation suggested by the implosive component of the deep 2013 Sea of Okhotsk earthquake, under the general concept of transformational faulting of metastable olivine. In this model, the phase transformation of metastable olivine is assumed to take place in the planar shear zone expressed by the deviatoric moment (Kirby, 1987). We use the simple model of a rectangular fault of length L and width W, the thickness of the zone undergoing the phase transformation being H.

If we assume a relative volume change $\alpha = -7.3\%$ (Jeanloz and Thompson, 1983) during a complete phase transformation in the zone, the total volume change will be $\delta V = \alpha (L \cdot W) \cdot H$, and the implosive moment release

$$M_I = K \cdot \delta V = K \cdot \alpha \cdot (L \cdot W) \cdot H \tag{4}$$

where K is the bulk modulus of the material, taken as 2.49×10^{12} dyn/cm^2 in the PREM model (Dziewonski and Anderson, 1981). Given the deviatoric moment $M_D = \mu \cdot (L \cdot W) \cdot \Delta u$, where μ is the rigidity and Δu the seismic slip on the fault, we obtain two expressions for H:

$$H = \frac{1}{\alpha \cdot K} \cdot \frac{M_I}{L \cdot W} = \Delta u \cdot \frac{1}{\alpha} \cdot \frac{\mu}{K} \cdot \frac{M_I}{M_D} \tag{5}$$

The first expression allows a direct estimate of H from M_I and the dimensions of the fault zone. A number of source tomography studies of the Sea of Okhotsk event suggest average values $L = 135$ km; $W = 50$ km (Wei et al., 2013; Ye et al., 2013; Zhan et al., 2014). This yields $H \approx 90$ cm, using $M_I = -1.1 \times 10^{27}$ dyn*cm as inverted from the radial modes, but up to 4 m for the source obtained by CMT inversions; we can retain an order of magnitude of 2 m. The second expression allows the direct scaling of H to the slip on the fault Δu through the dimensionless quantities α, M_I/M_D, and $\frac{\mu}{K} = \frac{1}{(V_P/V_S)^2 - 4/3} = \frac{3}{2} \cdot \frac{1-2\nu}{1+\nu}$, where ν is the material's Poisson ratio. Using the PREM value $\nu = 0.295$ (Dziewonski and Anderson, 1981), we obtain $\mu/K = 0.475$, and a ratio $R_1 = H/\Delta u \approx 0.17$ from the radial modes inversion, and 0.5 from the CMT solution. Note that R_1 does not depend on the exact values of L and W used to model the fault.

Shear zones of transformational faults produced experimentally in the laboratory offer some insights into their thicknesses in relation to

Table 3
Results of Moment Tensor Inversion Experiments: 1994 Bolivian event.

No.	Centroid				Inverted Moment Tensor							Best Double-Couple				M_I		ε	ε_D
	Lat. (°N)	Lon. (°E)	Depth (km)	Offset (s)	M_{rr}	$M_{\theta\theta}$	$M_{\phi\phi}$	$M_{r\theta}$	$M_{r\phi}$	$M_{\theta\phi}$	Residual	M_D	ϕ (°)	δ (°)	λ (°)		(%)†		
					1994 BOLIVIA: Short-Period Window 135–250 s														
19c	−13.89	−67.32	650	30.57	−0.784	0.820	−0.0360	−2.50	0.0539	−0.363	0.1354	2.65	311.0	11.5	−51.7	0			+0.02
20u	−13.89	−67.32	650	30.57	−0.773	0.833	−0.0223	−2.50	0.0540	−0.362	0.1354	2.65	310.9	11.5	−51.8	+0.0125	(+0.5)	+0.02	−0.023
					Standard Inversion 200–400 s														
21c	−13.91	−67.00	654	27.99	−0.935	0.859	0.0756	−3.34	0.215	−0.0763	0.0679	3.46	276.9	7.5	−86.9	0			−0.02
22u	−13.94	−67.01	651	27.97	−1.17	0.595	−0.221	−3.31	0.213	−0.0833	0.0675	3.43	277.6	7.5	−86.2	**−0.265**	(−7.7)	+0.06	−0.011
					Ultra-Long-Period Window 600–1200 s														
23c	−13.98	−68.24	655	31.54	−0.671	0.738	−0.0671	−3.08	0.0636	−0.308	0.3269	3.18	310.2	8.3	−51.7	0			+0.02
24u	−14.00	−68.24	654	31.53	−0.700	0.729	−0.0796	−3.08	0.0636	−0.308	0.3269	3.18	309.8	8.4	−52.1	−0.0169	(−0.5)	+0.03	−0.025

All moment values in units of 10^{28} dyn*cm.
† Value of M_I/M_D expressed in percent.

their shear displacements and fault lengths, albeit with some caveats. They exhibit the metrics of such faults at the very beginning of transformational fault nucleation, and faults that offset sample boundaries may not feature metrics directly comparable to those that would have developed in source regions tens of kilometers in scale, and then sheared and run freely. Experimental results reported in the literature include Burnley et al. (1991), who observed faulting offsets of 15–120 μm upon transformation of 1-μm grains in Mg_2GeO_4 ($R_1 = 0.01$–0.07), Green et al. (1990) in natural silicate olivine (10–30 μm offsets for 1-μm grains; $R_1 = 0.03$–0.1), and Kirby et al. (1992) in ice ($H = 20$ μm; $\Delta u = 1$ mm; $R_1 = 0.02$).

In addition, a recent study of transformational faulting in Mg_2GeO_4 also showed micrographic evidence of submicron fault thickness and of fine-grained spinel (Wang et al., 2017). These authors employed an array of ultrasonic transducers to demonstrate that their shear zones radiate elastic waves and hence propagate dynamically. They provided estimates of fault thickness of ~ 100 nm for a slip of ~ 1 μm, suggesting $R_1 \approx 0.1$, a value comparable to other laboratory experiments at much larger scales, as described above. Furthermore, Wang et al. (2017) used the waveforms recorded from these transducers to invert for the moment tensor of individual transformational faulting events, down to typical values of $M_0 \approx 100$ dyn*cm ($M_w \approx -9$). Although they publish histograms of the isotropic component of these moment tensors (with a slight preponderance of positive, *i.e.,* explosive events), their transducers were uncalibrated and their solutions may be less reliable than for the largest, best-recorded events of their previous study (Schubnel et al., 2013), conducted on significantly larger samples, and for which little if any isotropic component was reported.

In summary, and in very general terms, the values obtained in the present study, $R_1 = 0.17$–0.5, are somewhat higher than the reported experimental values, with which however they share a comparable order of magnitude. In this context, we note that ductile shear zones in crustal rocks tend to show an increase in fault thickness with total cumulative fault displacement and therefore that shear-zone thickness increases with increasing total displacement. If transformational faults in cold subducting lithosphere show similar scaling, one could anticipate that reactivation of transformational faults in the mantle transition zone would widen with increasing cumulative shear displacement and produce larger R_1 values than those observed in the experimental studies cited above.

This lends considerable support to our interpretation of the implosive component of the moment tensor as expressing the nucleation of transformational faulting, even though the earthquake and the laboratory experiments took place on geometric scales differing by 6–7 orders of magnitude, and in the case of ices, in materials of clearly different chemistry.

Another means of comparing our results from the 2013 Sea of Okhotsk earthquake to experimental ones would be to scale H to the fault length L, which amounts to defining the aspect ratio R_2 of the zone undergoing the phase transition. In this case, we find $R_2 \approx 1.5 \times 10^{-5}$, differing significantly from the laboratory experiments: Kirby et al. (1992) suggest $L = 2$ cm and hence $R_2 = 10^{-3}$, a figure also proposed by Wang et al. (2017), Green et al. (1990) suggest a failure extending over 3 mm, hence $R_2 = 3 \times 10^{-4}$; no information on length of faulting is available from Burnley et al. (1991). Note however that Wang et al. (2017) have observed that their fault thicknesses ($H \approx 100$ nm) may not scale directly with fault lengths L. This diversity in R_2 might express a variation in the strains released during transformational faulting, which are directly related to the ratios $\Delta u/L = R_2/R_1 \approx 10^{-4}$ in our case, but as much as 0.05 in Kirby et al.'s (1992) experiments on ices. Clearly, the latter figure would be excessive for an earthquake rupture: estimates of strain release during deep earthquakes, using energy-to-moment ratios have been found to be somewhat higher than for shallow sources, but only by less than one order of magnitude (Choy et al., 2006; Vallée, 2013; Saloor and Okal, 2018).
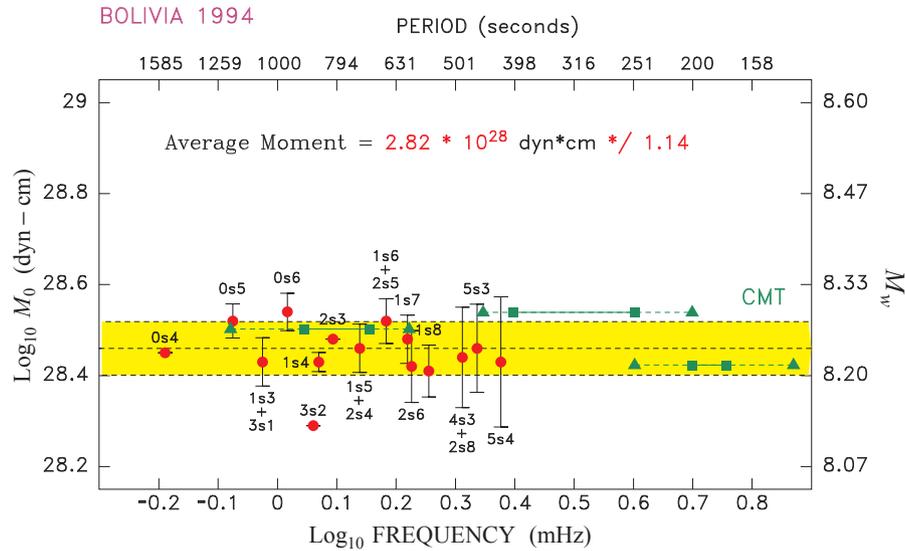
Fig. 5. Same as Fig. 2 for the 1994 Bolivian earthquake. Note again the absence of any trend in the normal mode dataset, but this time the irregular behavior of M_D from unconstrained CMT inversions, depending on the frequency band used. See text for details.

6. Discussion and conclusion

We have established by two independent methods that the source of the deep Sea of Okhotsk earthquake of 24 May 2013 included an implosive component, of an amplitude of between 3 and 8% of the deviatoric moment of the earthquake. CMT inversion results tentatively suggest a similar component of 5% of M_D for the recent 2015 Bonin earthquake. This result would be a natural consequence of transformational faulting as a mechanism of deep seismogenesis in the downgoing slab.

Ever since transformational faulting was suggested as a source of deep seismicity, its application to very large earthquakes, such as the 1994 Bolivian, and now the 2013 Okhotsk, events, has run into the argument that the inherently large size of their fault zones may not fit inside the relatively narrow domain of olivine metastability derived from thermal models (*e.g.,* Wiens et al., 1994; Silver et al., 1995; Myers et al., 1995; Tibi et al., 2003; Wei et al., 2013, Ye et al., 2013; Zhan et al., 2014; Zhang et al., 2016). However, a number of observations can reconcile the spatial extent of large earthquakes with the general concept of deep seismicity nucleating from transformational faulting: First, Green et al. (1992) have documented an experimental case in which the resulting crack extended outside the particular crystal involved in the phase transformation, suggesting that not all the seismic fault zone has to be contained inside the metastable wedge; in this context, Meng et al.'s (2014) recent suggestion, for the 2013 Okhotsk earthquake, of a fault zone extending outside the olivine wedge would not necessarily preclude transformational faulting. In addition, Chen (1995) had proposed, for the deep Bolivian earthquake, a model of discontinuous, *en échelon,* rupture leading to a transverse dimension (30 km) for the fault significantly narrower than inferred from the distribution of its aftershocks. Finally, the structure of the slab in the vicinity of the 660-km discontinuity is expected to be strongly perturbed from the simple thermal model used *e.g.,* by Kirby et al. (1996) to advocate nucleation and growth by transformational faulting. In several subduction zones, the slab has been mapped, either by tomography or precise relocation of seismicity, to be horizontally deflected and thickened as it reaches the bottom of the transition zone, *e.g.,* in the Izu-Bonin system (Fukao et al., 1992) or in Tonga (van der Hilst, 1995; Okal and Kirby, 1998). This thickening is due to down-dip compression of the slab as it encounters resistance to penetration caused by the strong viscosity contrast at the discontinuity and by the buoyancy cost of metastable olivine attempting to penetrate the lower mantle (Kirby

et al., 1996; Bina, 1997; Okal and Kirby, 1998), and it would argue for a metastable wedge of larger dimensions than in simplified models such as Kirby et al.'s (1996). More generally, slabs are complex, internally deformed regions, which can feature significant heterogeneity in their history, and hence in their mineralogical and thermal structures, a classical example being the plate age discontinuity "memorized" into the South American slab as a result of a reorganization of plate boundaries at around 82 Ma (Engebretson and Kirby, 1992).

In the context of the 2013 Sea of Okhotsk earthquake, the geometry of the slab was poorly mapped prior to the event due to the scarcity of background seismicity, and in this respect the local details of the Slab1.0 model (Hayes et al., 2012), and hence the estimated location and size of the metastable wedge, may have some uncertainty, as suggested by the distribution of 2013 aftershocks (Zhan et al., 2014). Most source models (Tsuboi et al., 2013; Ye et al., 2013; Zhan et al., 2014) favor rupture along a very shallow dipping fault plane ($\delta \sim 10°$) which might be contained inside the olivine wedge if the slab is locally deflected to a sub-horizontal geometry (Wei et al., 2013). Note however that some competing models would favor rupture along the sub-vertical fault plane, or stacking of *en échelon* horizontal rupture segments along a vertical extent reaching 40 km (Chen et al., 2014; Zhang et al., 2016). One possible re-interpretation of these observations would be that the slab deviates from the Slab1.0 model by striking essentially North-South and being deflected sub-horizontally (Wei et al., 2013; Figs. 1A and 3a). This geometry would be consistent with the GlobalCMT focal mechanism ($\phi = 189°; \delta = 11°; \lambda = -93°$). A rupture propagating from the hypocenter southwards, essentially parallel to the strike and across a sub-horizontal width of ~ 50 km may be contained inside the olivine wedge of a locally deflected slab, thus vitiating the argument against transformational faulting as a process nucleating large deep earthquakes and controlling their rupture.

It is also noteworthy that the 2013 deep Okhotsk earthquake took place at the Northeastern end of the Kuril-Kamchatka subduction system, and thus followed the trend identified by Kirby et al. (1996) that the largest deep earthquakes occur near the local spatial (including lateral) limits of Wadati-Benioff zones. These authors attributed this pattern to internal or "self" stresses generated, upon transformation, by the effects of heterogeneous volume changes and by significant gradients in the structural and elastic properties of the material composing the slabs (Goto et al., 1987; Kirby et al., 1991); such gradients would be enhanced at the lateral limits of a seismogenic metastable wedge.

In conclusion, our study opens a significant new chapter in the 45-

year old controversy about the observation of implosive components in deep earthquakes. We now have proof that the largest such event ever recorded, the 2013 Sea of Okhotsk earthquake, featured a detectable implosive component. However, the next two runner-ups in terms of moment, the 1994 Bolivian and 1970 Colombian earthquake, when subjected to modern, careful studies, failed to exhibit similar evidence (Hara et al., 1995; Okal, 1996; Russakoff et al., 1997), as did the many smaller shocks studied by Kawakatsu (1991a). This situation remains intriguing and deserves further discussion.

We note that under the model of transformational faulting, the phase transformation expressed as the implosive moment tensor component M_I serves as a nucleation and growth process for the faulting. Overwhelming evidence, going back to Isacks and Molnar (1971) and upheld by countless studies based on the more modern GlobalCMT solutions, indicates that such faulting releases slab stresses featuring spatial coherence and successfully interpreted in the framework of plate tectonics as down-dip compressional stresses resulting from the resistance to penetration of the deep mantle encountered by the slab as it approaches the 660-km discontinuity (with the exception of chunks of subducted material mechanically detached from their slab, and recumbent on the bottom of the transition zone, as evidenced by Okal and Kirby (1998) under the Fiji Basin). In this framework, the phase transformation and the main episode of faulting draw their energies from different reservoirs, and there may not necessarily be a direct scaling between by their relative sizes, which would be expressed as an invariant ratio between M_I and M_D. This would be supported, *e.g.,* by the scatter in the ratio R_1 computed from Burnley et al.'s (1991) experiments.

Fig. 4 shows that the 1994 Bolivian event could not have included an implosive component of the same size, relative to $M_D \cdot s_R$, as for the 2013 Okhotsk earthquake, which would have amounted to $M_I = -3.0 \times 10^{26}$ dyn*cm if referred to our radial mode solution, and $M_I = -1.2 \times 10^{27}$ dyn*cm using the CMT one; such values would plot outside the relevant confidence ellipse. On the other hand, the Bolivian event could have included an isotropic component scaling on the lower end of the laboratory values, say $R_1 = 0.02$, since the corresponding value of M_I would have been only -8×10^{25} dyn*cm, which would fit inside the ellipse on Fig. 4, meaning that the data analyzed by Okal (1996) could not exclude it. Thus, the detection of an isotropic component in 2013 and its absence in 1994 could be a result of a scatter in values of R_1, *i.e.,* in the ratio of the isotropic to deviatoric moments, which may itself express a difference in slab environment, perhaps traceable to plate kinematics, affecting the rupture process of large deep earthquakes, as suggested *e.g.,* by Wiens and McGuire (1995), Lundgren and Giardini (1995), and more recently Zhan et al. (2014).

In this general framework, the quantitative examination of the laboratory results, including those of Green et al. (1990) which come closest to reproducing the conditions inside the slab (but for the absence of externally applied stresses), would suggest that the amplitude of the isotropic component could in the majority of cases be so small relative to its deviatoric counterpart as to prevent its detection, including by methods such as the spectral ratio of radial modes used in the present study, which are supposed to optimize such detection. In the general context of Okal and Geller's (1979) conclusions, this would have made it impossible to detect any putative isotropic component to the source of the 1994 Bolivian earthquake, despite the advent of digital data allowing the resolution of radial mode spectra, a task clearly impossible using the analog data of the 1970s. It is probably along this framework that the apparently contradictory results on the 1970 Colombian, 1994 Bolivian and 2013 Sea of Okhotsk sources can be reconciled and the isotropic source controversy resolved.

Acknowledgments

References

Bina, C.R., 1997. Patterns of deep seismicity reflect buoyancy stresses due to phase transitions. Geophys. Res. Lett. 24, 3381–3386.

Bridgman, P.W., 1945. Polymorphic phase transitions and geological phenomena. Am. J. Sci. 243A, 90–97.

Burnley, P.C., Green II, H.W., Prior, D., 1991. Faulting associated with the olivine-to-spinel transformation in Mg_2GeO_4 and its application for deep-focus earthquakes. J. Geophys. Res. 96, 425–443.

Chen, W.-P., 1995. En échelon ruptures during the great Bolivian earthquake of 1994. Geophys. Res. Lett. 22, 2261–2264.

Chen, Y., Wen, L., Ji, C., 2014. A cascading failure during the 24 May 2013 great Okhotsk deep earthquake. J. Geophys. Res. 119, 3035–3049.

Choy, G.L., McGarr, A., Kirby, S.H., Boatwright, J., 2006. An overview of the global variability in radiated energy and apparent stress. Am. Geophys. Un. Geophys. Monog. 170, 43–57.

Čížková, H., Bina, C.R., 2015. Geodynamics of trench advance: insights from a Philippine-Sea-style geometry. Earth Planet. Sci. Lett. 430, 408–415.

Dahlen, F.A., 1982. The effect of data windows on the estimation of free oscillation parameters. Geophys. J. R. Astr. Soc. 69, 537–549.

Dahlen, F.A., Sailor, R.V., 1979. Rotational and elliptical splitting of the free oscillations of the Earth. Geophys. J. R. Astr. Soc. 58, 609–623.

Dziewonski, A.M., Anderson, D.L., 1981. Preliminary reference Earth model. Phys. Earth Planet. Inter. 25, 297–356.

Dziewonski, A.M., Chou, T.A., Woodhouse, J.H., 1981. Determination of earthquake source parameters from waveform data for studies of global and regional seismicity. J. Geophys. Res. 86, 2825–2852.

Ekström, G., Nettles, M., Dziewoński, A.M., 2012. The global CMT project, 2004–2010: centroid moment tensors for 13,107 earthquakes. Phys. Earth Planet. Inter. 200, 1–9.

Engebretson, D., Kirby, S.H., 1992. Deep Nazca slab seismicity: why is it so anomalous? EOS Trans. Am. Geophys. Union 73 (43), 379 [abstract].

Fukao, Y., Osayabashi, M., Inoue, H., Nenbai, M., 1992. Subducting slabs stagnant in the mantle transition zone. J. Geophys. Res. 97, 4809–4822.

Gilbert, J.F., 1971. Excitation of the normal modes of the Earth by earthquake sources. Geophys. J. R. Astr. Soc. 22, 223–226.

Gilbert, J.F., Dziewonski, A.M., 1975. An application of normal mode theory to the retrieval of structural parameters and source mechanisms from seismic spectra. Philos. Trans. R. Soc. London 278A, 187–269.

Goto, K., Suzuki, Z., Hamguchi, H., 1987. Stress distribution due to olivine-spinel phase transition in descending plate and deep focus earthquakes. J. Geophys. Res. 92, 13811–13820.

Green II, H.W., Burnley, P.C., 1989. A new self-organizing mechanism for deep earthquakes. Nature 341, 733–737.

Green II, H.W., Young, T.E., Walker, D., Scholz, C.H., 1990. Anti-crack associated faulting at very high pressure in natural olivine. Nature 348, 720–722.

Green II, H.W., Scholz, C.H., Tingle, T.N., Young, T.E., Koczynski, T.A., 1992. Acoustic emissions produced by anticrack faulting during the olivine→spinel transformation. Geophys. Res. Lett. 19, 789–792.

Hara, T., Kawakatsu, H., 2016. Full moment tensor inversion for the large deep earthquakes. Proc. Japan Geoscience Un. Mtg. SCG20-05, Chiba [abstract].

Hara, T., Kuge, K., Kawakatsu, H., 1995. Determination of the isotropic component of the 1994 Bolivia deep earthquake. Geophys. Res. Lett. 22, 2265–2268.

Hayes, G.P., Wald, D.J., Johnson, R.L., 2012. Slab1.0: a three-dimensional model of global subduction zone geometries. J. Geophys. Res. 117 (B1), B01302 15p.

Isacks, B.L., Molnar, P., 1971. Distribution of stresses in the descending lithosphere from a global survey of focal-mechanism solutions of mantle earthquakes. Revs. Geophys. Space Phys. 9, 103–174.

Jeanloz, R., Thompson, A.B., 1983. Phase transitions and mantle discontinuities. Rev. Geophys. Space Phys. 21, 51–74.

Jeffreys, H., 1924. The Earth: Its Origin, History and Physical Constitution. Cambridge Univ Press 278 p.

Jiang, G., Zhao, D., Zhang, G., 2015. Detection of metastable olivine wedge in the Western Pacific slab and its geodynamic implications. Phys. Earth Planet. Inter. 238, 1–7.

Kagan, Y.Y., 1991. 3-D rotation of double-couple earthquake sources. Geophys. J. Int. 106, 709–716.

Kanamori, H., Cipar, J.J., 1974. Focal process of the great Chilean earthquake, May 22, 1960. Phys. Earth Planet. Inter. 9, 128–136.

Kaneshima, S., Okamoto, T., Takenaka, H., 2007. Evidence for a metastable olivine wedge inside the subducted Mariana slab. Earth Planet. Sci. Lett. 258, 219–227.

Kawasaki, I., Tanimoto, T., 1981. Radiation patterns of body waves due to the seismic dislocation occurring in an anisotropic source medium. Bull. Seismol. Soc. Am. 71, 37–50.

Kawakatsu, H., 1991a. Insignificant isotropic component in the moment tensor of deep earthquakes. Nature 351, 50–53.

Kawakatsu, H., 1991b. Enigma of earthquakes at ridge-transform-fault plate boundaries: distribution of non-double-couple parameter of Harvard CMT solutions. Geophys. Res. Lett. 18, 1103–1106.

Kawakatsu, H., 1996. Observability of the isotropic component of a moment tensor. Geophys. J. Int. 126, 525–544.

Kawakatsu, H., Yoshioka, S., 2011. Metastable olivine wedge and deep dry cold slab beneath SW Japan. Earth Plan. Sci. Lett. 303, 1–10.

Kikuchi, M., Kanamori, H., 1994. The mechanism of the deep Bolivia earthquake of June 9, 1994. Geophys. Res. Lett. 21, 2341–2344.

Kirby, S.H., 1987. Localized polymorphic phase transformations in high-pressure faults and applications to the physical mechanism of deep earthquakes. J. Geophys. Res. 92, 13789–13800.

Kirby, S.H., Durham, W.B., Stern, L.A., 1991. Mantle phase changes and deep-earthquake faulting in subducting lithosphere. Science 252, 216–225.

Kirby, S.H., Durham, W.B., Stern, L.A., 1992. The Ice I → Ice II transformation: mechanisms and kinetics under hydrostatic and non-hydrostatic conditions. In: Maeno, N., Hondoh, T. (Eds.), Physics and Chemistry of Ice. Hokkaido Univ. Press, Sapporo, pp. 456–463.

Kirby, S.H., Stein, S., Okal, E.A., Rubie, D., 1996. Deep earthquakes and metastable mantle phase transformations in subducting oceanic lithosphere. Rev. Geophys. Space Phys. 34, 261–306.

Leith, A., Sharpe, J.A., 1936. Deep-focus earthquakes and their geological significance. J. Geol. 44, 877–917.

Lundgren, P.R., Giardini, D., 1995. The June 9 Bolivia and March 9 Fiji deep earthquakes of 1994: 1. Source processes. Geophys. Res. Lett. 22, 2241–2244.

Mainka, C., 1915. Über Zeitdifferenzen aufallender Einsätze in einem Seismogramm gegen den ersten. Gerlands Beitr. z. Geophys. 14, 39–84.

Meng, L., Ampuero, J.-P., Bürgmann, R., 2014. The 2013 Okhotsk deep-focus earthquake: rupture beyond the metastable olivine wedge and thermally controlled rise time near the edge of a slab. Geophys. Res. Lett. 41, 3779–3785.

Millot-Langet, R., 2004. Modélisation des modes propres et des sismogrammes longue-période d'une Terre anélastique en rotation. Inst. Phys. Globe Paris 190 p. (Thèse de Doctorat).

Myers, S.C., Wallace, T.C., Beck, S.L., Silver, P.G., Zandt, G., Vandecar, J., Minaya, E., 1995. Implications of spatial and temporal development of the aftershock sequence for the $M_w = 8.3$ June 9, 1994 deep Bolivian earthquake. Geophys. Res. Lett. 22, 2269–2272.

Okal, E.A., 1978. A physical classification of the Earth's spheroidal modes. J. Phys. Earth 26, 75–103.

Okal, E.A., 1996. Radial modes from the great 1994 Bolivian earthquake: no evidence of an isotropic component to the source. Geophys. Res. Lett. 23, 431–434.

Okal, E.A., 2001. Detached deep earthquakes: are they really? Phys. Earth Planet. Inter. 127, 109–143.

Okal, E.A., 2013. From 3–Hz P waves to $_0S_2$: No evidence of a slow component to the source of the 2011 Tohoku earthquake. Pure Appl. Geophys. 170, 963–973.

Okal, E.A., Geller, R.J., 1979. On the observability of isotropic seismic sources: the July 31, 1970 Colombian earthquake. Phys. Earth Planet. Inter. 18, 176–196.

Okal, E.A., Kirby, S.H., 1998. Deep earthquakes beneath the North and South Fiji Basins, SW Pacific: Earth's most intense deep seismicity in stagnant slabs. Phys. Earth Planet. Inter. 109, 25–63.

Okal, E.A., Kirby, S.H., 2016. The large Bonin deep event of 30 May 2015: Seismogenesis in a detached and fragmented slab. Geophys. Res. Abstracts 18, EGU2016-10715 [abstract].

Okal, E.A., Stein, S., 2009. Observations of ultra-long period normal modes from the 2004 Sumatra-Andaman earthquake. Phys. Earth Planet. Inter. 175, 53–62.

Okal, E.A., Hongsresawat, S., Stein, S., 2012. Split mode evidence for no ultra-slow component to the source of the 2010 Maule, Chile earthquake. Bull. Seismol. Soc. Am. 102, 391–397.

Pilgrim, L., 1913. Die Berechnung der Laufzeiten eines Erdstosses mit Berücksichtigung der Herdtiefen, getstützt auf neurere Beobachtungen. Gerlands Beitr. z. Geophys. 12, 363–483.

Russakoff, D., Ekström, Tromp, J., 1997. A new analysis of the great 1970 Colombia earthquake and its isotropic component. J. Geophys. Res. 102, 20423–20434.

Saloor, N., Okal, E.A., 2018. Extension of the energy-to-moment parameter Θ to intermediate and deep earthquakes. Phys. Earth Planet. Inter. 274, 37–48.

Schubnel, A., Brunet, F., Hilairet, N., Gasc, J., Wang, Y., Green II, H.W., 2013. Deep-focus earthquake analogs recorded at high pressure and temperature in the laboratory. Science 341, 1377–1380.

Silver, P.G., Beck, S.L., Wallace, T.C., Meade, C., Myers, S.C., James, D.E., Kuehnel, R., 1995. Rupture characteristics of the deep Bolivian earthquake of 9 June 1994 and the mechanism of deep-focus earthquakes. Science 268, 69–73.

Stechschulte, V.C., 1932. The Japanese earthquake of March 29, 1928, and the problem of depth of focus. Bull. Seismol. Soc. Am. 22, 81–137.

Stein, S., Geller, R.J., 1977. Amplitudes of the Earth's split normal modes. J. Phys. Earth 25, 117–142.

Stein, S., Okal, E.A., 2005. Size and speed of the Sumatra earthquake. Nature 434, 581–582.

Tibi, R., Bock, G., Wiens, D.A., 2003. Source characteristics of large deep earthquakes: constraint on the faulting mechanism at great depths. J. Geophys. Res. 108 (B2), B001948 25p.

Tsuboi, S., Miyoshi, T., Nakamura, T., Obayashi, M., Tono, Y., 2013. Source mechanism of May 24, 2013 Sea of Okhotsk deep earthquake ($M_w = 8.3$) estimated by broadband waveform modeling. EOS Trans. Am. Geophys. Union 94 (53) S41C-07 [abstract].

Turner, H.H., 1922. On the arrival of earthquake waves at the antipodes, and on the measurement of the focal depth of the earthquake. Mon. Not. R. Astr. Soc. Geophys. Supp. 1, 1–13.

Vaišnys, J.R., Pilbeam, C.C., 1976. Deep-earthquake initiation by phase transformation. J. Geophys. Res. 81, 985–988.

Vallée, M., 2013. Source time function properties indicate a strain drop independent of earthquake depth and magnitude. Nat. Commun. 4, 2606 6p.

van der Hilst, R.D., 1995. Complex morphology of subducted lithosphere in the mantle beneath the Tonga trench. Nature 374, 154–157.

Vavryčuk, V., 2004. Inversion for anisotropy from non-double-couple components of moment tensors. J. Geophys. Res. 109 (B7), B07306 13p.

Vavryčuk, V., 2005. Focal mechanisms in anisotropic media. Geophys. J. Int. 161, 334–346.

Wadati, K., 1927. Existence and study of deep earthquakes. J. Meteorol. Soc. Jpn. Ser. 2 (5), 119–145 (in Japanese).

Wadati, K., 1928. Shallow and deep earthquakes. Geophys. Mag. 1, 161–202.

Wadati, K., 1929. Shallow and deep earthquakes (2nd paper). Geophys. Mag. 1, 1–36.

Wang, Y., Zhu, L., Shi, F., Schubnel, A., Hilairet, N., Yu, T., Rivers, M., Gasc, J., Addad, A., Deldicque, D., Li, Z., Brunet, F., 2017. A laboratory nanoseismological study on deep-focus earthquake micromechanics. Sci. Adv. 3, e1601896 12p.

Wei, S., Helmberger, D.V., Zhan, Z., Graves, R., 2013. Rupture complexity of the $M_w = 8.3$ Sea of Okhotsk earthquake: rapid triggering of complementary earthquakes? Geophys. Res. Lett. 40, 5034–5039.

Wiens, D.A., McGuire, J.J., Shore, P.G., Bevis, M.G., Draunidalo, K., Prasad, G., Helu, S.P., 1994. A deep earthquake aftershock sequence and implications for the rupture mechanism of deep earthquakes. Nature 372, 540–543.

Wiens, D.A., McGuire, J.J., 1995. 1994 Bolivia and Tonga events: fundamentally different types of deep earthquakes? Geophys. Res. Lett. 22, 2245–2248.

Woodhouse, J.H., 1980. The coupling and attenuation of nearly resonant multiplets in the Earth's free oscillation spectrum. Geophys. J. R. Astr. Soc. 61, 261–283.

Ye, L., Lay, T., Kanamori, H., Koper, K.D., 2013. Energy release of the 2013 $M_w = 8.3$ Sea of Okhotsk earthquake and deep slab stress heterogeneity. Science 341, 1380–1384.

Ye, L., Lay, T., Zhan, Z., Kanamori, H., Hao, J.-L., 2016. The isolated ~ 680-km deep 30 May 2015 $M_w = 7.9$ Ogasawara (Bonin) Islands earthquake. Earth Planet. Sci. Lett. 433, 169–179.

Zhan, Z., Kanamori, H., Tsai, V.C., Helmberger, D.V., Wei, S., 2014. Rupture complexity of the 1994 Bolivia and 2013 Sea of Okhotsk deep earthquakes. Earth Planet. Sci. Lett. 385, 89–96.

Zhang, H., van der Lee, S., Bina, C.R., Ge, Z., 2016. Rupture mechanism of the May 24, 2013 $M_w = 8.3$ Sea of Okhotsk deep-focus earthquake. Seismol. Res. Lett. 87, 543–544 (abstract).

Zhao, D., Fujisawa, M., Tyokuni, G., 2017. Tomography of the subducting Pacific slab and the 2015 Bonin deepest earthquake ($M_w = 7.9$). Sci. Rep. 7, 44487 8p.